The Canadian Mineralogist
Vol. 36, pp. 1595-1605 (1998)

TEM AND XRD STUDY OF ANTIGORITE SUPERSTRUCTURES

SEIICHIRO UEHARA[1]

Department of Earth and Planetary Sciences, Faculty of Science, 33, Kyushu University, Hakozaki, 6-10-1 Fukuoka, 812-8581, Japan

Abstract

Samples of antigorite exhibiting variety in superstructures, taken from low-grade to high-grade serpentinites from southwestern Japan, were studied by X-ray diffraction (XRD), selected-area electron diffraction (SAED), and high-resolution transmission electron microscopy (HRTEM). Indexed XRD patterns indicate an A cell parameter of the supercell in the range 35.4 – 53.6 Å, and the following dimensions of the subcell: $5.407 < a < 5.466$, $9.238 < b < 9.262$, $7.241 < c < 7.279$ Å, $91.07 < \beta < 91.65°$. SAED patterns show a wider range of A parameters, from 28 to 61 Å ($5.0 < M < 11.4$, $M = A/a$). Antigorite with a 40.0 – 42.5 Å supercell ($M = 7.5$) is the common structure in southwestern Japan. A new method for supercell measurement by powder XRD is proposed. M values show a linear relation with the XRD-derived parameter, $\Delta 2\theta$: $M = 14.26 - 2.41\ \Delta 2\theta$. A sample of antigorite with $A = 43$ Å ($M = 8$) belongs to space group *Pm*. Diffraction patterns (single-crystal XRD and SAED) and c-axis HRTEM images of antigorite having $M = (2n + 1)/2$ indicate that the true periodicity of the superstructure along the X direction is $2A$, corresponding to two waves, and the space lattice is C-centered.

Keywords: antigorite, XRD, SAED, HRTEM, supercell, superstructure, Japan.

Sommaire

Des échantillons d'antigorite montrant une variété de surstructures, prélevés de serpentinites du sud-ouest du Japon dont le degré de métamorphisme va de faible à élevé, ont été caractérisés par diffraction X, diffraction d'électrons sur aire restreinte, et par microscopie électronique par transmission à haute résolution. Une indexation du spectre de diffraction X mène au paramètre A de la surstructure, dans l'intervalle 35.4 – 53.6 Å, et aux paramètres réticulaires suivants de la sous-structure: $5.407 < a < 5.466$, $9.238 < b < 9.262$, $7.241 < c < 7.279$ Å, $91.07 < \beta < 91.65°$. Les clichés de diffraction d'électrons révèlent un intervalle plus grand du paramètre A, entre 28 et 61 Å ($5.0 < M < 11.4$, $M = A/a$). L'antigorite ayant une maille de 40.0 à 42.5 Å ($M = 7.5$) est la structure la plus courante dans le sud-ouest du Japon. Ce travail contient la description d'une nouvelle méthode pour déterminer la surstructure à partir du spectre de diffraction X obtenu sur poudre. Les valeurs de M montrent une relation linéaire avec le paramètre $\Delta 2\theta$ dérivé par diffraction X: $M = 14.26 - 2.41\ \Delta 2\theta$. Un échantillon d'antigorite ayant A égal à 43 Å ($M = 8$) répond au groupe spatial *Pm*. Les spectres de diffraction sur cristaux uniques (diffraction X aussi bien que diffraction d'électrons) et les images de la structure de l'antigorite dans laquelle $M = (2n + 1)/2$, obtenues à haute résolution et montrant la périodicité le long de c, prouvent que la vraie périodicité de la surstructure le long de la direction X est $2A$, ce qui correspond à deux ondes, et le réseau est centré sur C.

(Traduit par la Rédaction)

Mots-clés: antigorite, diffraction X, diffraction d'électrons sur aire restreinte, microscopie par transmission à haute résolution, surmaille, surstructure, Japon.

Introduction

Antigorite is characterized by a large superstructure along the [100] direction. Zussman (1954) suggested, on the basis of X-ray and optical diffraction patterns and images, that the superstructure is a result of a repeating wave structure, either of the rectified or alternating type. The alternating-wave structure was investigated by Kunze (1956, 1958, 1961). In this paper, "A" is used for the supercell repeat-unit in antigorite, whereas "a" is used for the subcell repeat-unit, about 5.4 Å. The A parameter of antigorite was shown by Aruja (1945) to be 43.5 Å, about eight times larger than the ideal, on a specimen from Mikonui, New Zealand, studied by X-ray rotation diagrams. The indexing of the powder pattern of antigorite based on the unit cell (A 43.38, b 9.257, c 7.270 Å, β 91.40°) of Aruja (1945) was made by Whittaker & Zussman (1956).

[1] *E-mail address*: uehara@geo.kyushu-u.ac.jp

Uehara & Shirozu (1985) defined the superstructure in terms of the number (M) of subcells (a = 5.44 Å) along X; thus $M = A/a$. This defines the superstructure in terms of the number of octahedra present (two per subcell) along X, and not the tetrahedra. The M of Uehara & Shirozu is related to the m of Kunze by the relation of $M = (m - 1)/2$. Uehara & Shirozu (1985) showed, on the basis of X-ray- and electron-diffraction studies, that samples of antigorite may be classified into three structural types. In the first structure, $M = n$ (where n is an integer), in the second type, $M = (2n + 1)/2$, and in the third type, $M \neq n/2$. The first type contains an odd number of tetrahedra (m) and an even number of octahedra (m–1) in the superstructure period A with the space group Pm. The second type has a structure derived from the first type, but different from the structure proposed by Kunze (1961), with m = even and space group $P2/m$. The model based on $M = (2n + 1)/2$ is obtained by shifting of Kunze's model at each wave unit along Y by $b/2$. The model has a repeat period of $2A$ with a C-centered space lattice. The model contains an even number of tetrahedra (m) and an odd number of octahedra ($m - 1$). The third structure $M \neq n/2$ is a mixture of the above two structures in coherent domains, and it is commonly found in poorly crystallized, disordered material.

Some samples of antigorite (Spinnler 1985, Mellini *et al.* 1987, Otten 1993) have an "offset" in selected-area electron-diffraction patterns caused by a noncoincidence of the X^* vectors in the supercell and subcell. The offsets in selected-area electron-diffraction patterns occur because of differences in orientation between the subcell and supercell, resulting in an average multilayer unit-cell. The structure is analogous to an incommensurate modulated structure such as in e-plagioclase.

Electron optical studies (*e.g.*, Zussman *et al.* 1957, Kunze 1961) of various specimens of antigorite showed that the A cell length ranges from 16 to 110 Å, with most values between 33 and 44 Å. These values were obtained by electron diffraction or lattice images. However, X-ray-diffraction techniques were not used to obtain supercell spacings until Uehara & Shirozu (1985) showed that they could obtain accurate values for even small variations in values of d.

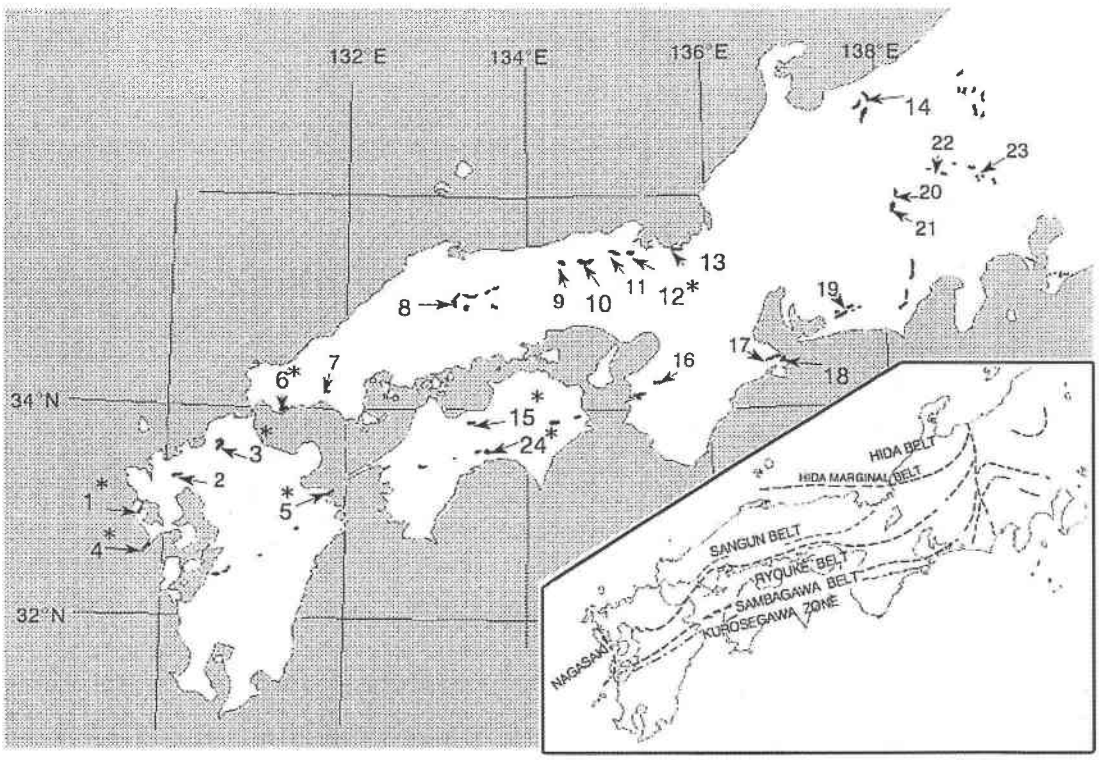

FIG. 1. Distribution of serpentinites in southwestern Japan, modified after Hashimoto *et al.* (1970). Asterisks mark localities from which antigorite was described in this study: 1 Nishisonogi, 2 Kyuragi, 3 Sasaguri, 4 Nomo, 5 Saganoseki, 6 Ube, 7 Deai, 8 Tari, 9 Wakasa, 10 Sekinomiya, 11 Izushi, 12 Oeyama, 13 Oshima, 14 Happo-One, 15 Higashiakaishi, 16 Kinokawa, 17 Iseshi, 18 Toba, 19 Uhu, 20 Chino, 21 Oogawara-Irisawai, 22 Kurouchi-yama, 23 Kanasaki, and 24 Kochi.

This study concerns samples of antigorite from low- to high-grade metamorphic serpentinites found in southwestern Japan, characterized by transmission electron microscopy (TEM) and X-ray diffraction (XRD). The results, along with previously reported results on antigorite from Sasaguri, Nishisonogi and Saganoseki (Uehara & Shirozu 1985, Uehara 1987, Uehara & Kamata 1994) are discussed. Supercell values obtained by TEM and XRD are compared, and a new method for the measurement of the supercell parameter is given. HRTEM is used for a structure analysis of antigorite with a model type of $M = (2n + 1)/2$ type.

Materials and Experimental

The distribution of serpentinite bodies in southwestern Japan and sampling sites are shown in Figure 1. Serpentinites occur in the Sangun metamorphic belt (localities 2 – 13 in Fig. 1), the Sanbagawa metamorphic belt (5, 15 –23), the Kurosegawa belt (17, 18, 24), the Hida belt (14) and the Nagasaki metamorphic rocks (1, 4). These metamorphic belts belong to high-pressure intermediate type of metamorphism (Miyashiro 1961). Later (Cretaceous) emplacement of granitic rocks also induced thermal metamorphism of serpentines in the Sangun belt.

Identification by XRD of the serpentine species, antigorite, lizardite and chrysotile, relied on the powder data of Whittaker & Zussman (1956). The nomenclature of chrysotile polytypes follows the notation of Wicks & Whittaker (1975). Lizardite is predominant in our samples. The occurrence of antigorite is locally important in the Sangun and Hida serpentinites (locality 2–13, 14 in Fig. 1), whereas antigorite is the principal serpentine mineral in the Sanbagawa and Nagasaki serpentinites.

Antigorite from Sasaguri (#3 in Fig. 1), Nishisonogi (#1), Oeyama (#12) and Saganoseki (#5) was reported on in Uehara & Shirozu (1985), Uehara (1987) and Uehara & Kamata (1994). The antigorite samples investigated here were obtained mainly from Alpine-type serpentinites of the epidote-amphibolite-facies metamorphic rocks of the Nomo area, Nagasaki Prefecture

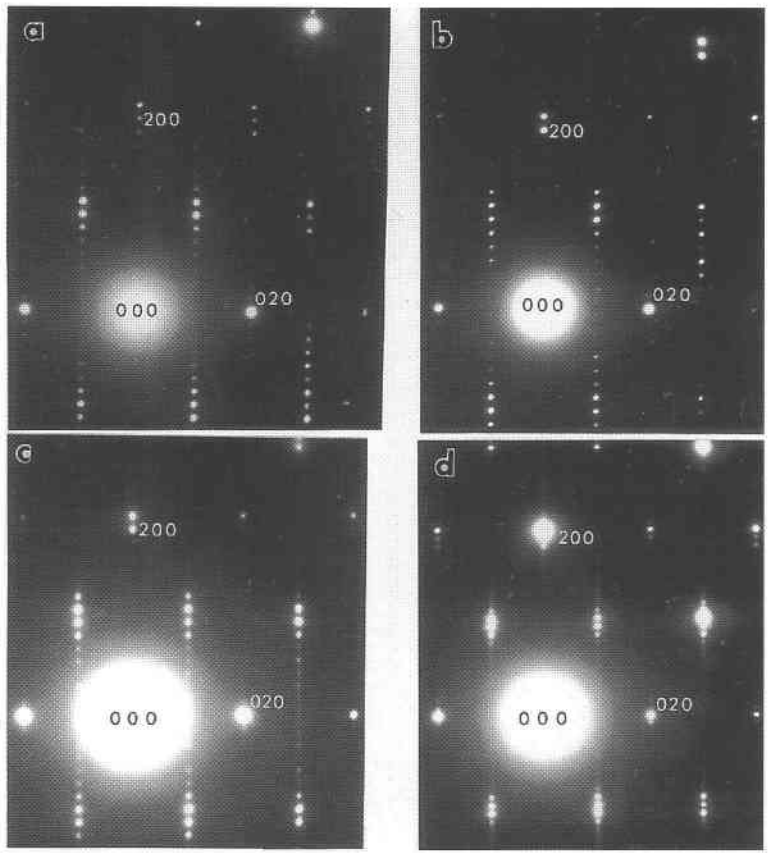

FIG. 2. *hk*0 SAED patterns of antigorite with (a) $M = 7.0$, (b) $M = 6.5$, (c) $M = 7.2$, and (d) $M = 11.4$.

(#4), the amphibolite- or greenschist-facies metamorphic rocks of the Bessi area, Ehime Prefecture (#15), the greenschist-facies rocks of the Ube area, Yamaguchi Prefecture (#6), and the prehnite–pumpellyite-facies rocks of Yokokurayama, Kochi Prefecture (#24). Four samples from Sasaguri (A2, A6) and Nishisonogi (N26, N55E) also were investigated. Electron-microprobe analyses of three specimens (A2, N26, N55E) showed considerable chemical heterogeneity in Fe and Mg contents.

Powder XRD patterns were recorded with a Rigaku RAD–IIA diffractometer using Ni-filtered Cu$K\alpha$ radiation and a standard aluminum sample holder. Slow scanning at 1/16° 2θ/min and a chart speed of 2.5 mm/min were used to achieve resolution of many closely spaced peaks. Silicon powder was used as an internal standard.

Electron optical observations were made with JEOL JEM–200B, JEM–2000FX and JEM–4000EX electron microscopes in the HVEM laboratory of Kyushu University. The JEM–200B microscope, which was primarily used to obtain selected-area electron-diffraction patterns, was operated at 200 kV. A selected-area aperture of 10 μm diameter was used, which has a projected diameter on the specimen of about 0.2 μm. HRTEM images were obtained at 200 kV with the JEM–2000FX and at 400 kV with the JEM–4000EX.

The JEOL JEM–4000EX is a top-entry electron microscope with a double-tilt sample holder capable of 25% tilts. The microscope has a structure-resolution limit of 1.7 Å, a spherical aberration coefficient of 1.0 mm, and chromatic aberration coefficient of 1.9 mm. A 50 μm objective aperture and a 200 μm condenser aperture were used for HRTEM imaging at 400 kV accelerating voltage. The simulated images of antigorite were calculated using the CIHRTEM computer program (Horiuchi & Matsui 1983). More detailed information concerning HRTEM imaging is given by Uehara (1994).

The pulverized samples were disaggregated by ultrasonic means and mounted on a microgrid or collodion film on copper specimen grids. Some antigorite specimens were ion-thinned to investigate texture and for crystal-structure analysis.

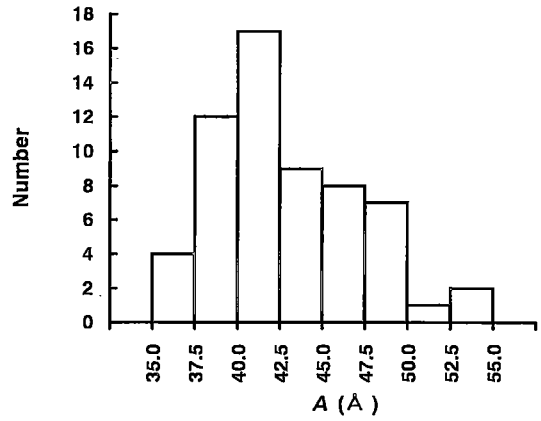

FIG. 3. Histogram for supercell parameter of antigorite in southwestern Japan obtained by powder XRD.

RESULTS AND DISCUSSION

Supercell obtained by powder XRD and SAED

The powder XRD patterns of the samples studied were indexed following the procedures of Uehara & Shirozu (1985). As with the earlier samples (Uehara & Shirozu 1985, Uehara & Kamata 1994), the *A* parameter was found to be in the range 35.4 – 53.6 Å, and subcell dimensions were in the ranges *a* 5.407 – 5.466, *b* 9.238 – 9.262, *c* 7.241 – 7.279 Å, β 91.07 – 91.65°. These parameters (Table 1) were obtained by the least-

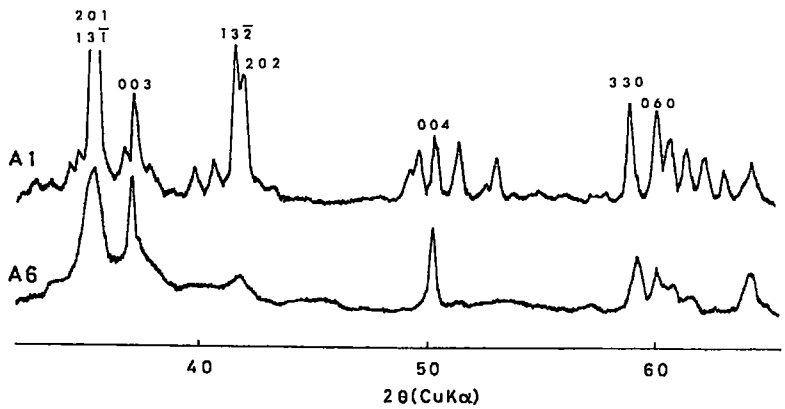

FIG. 4. Powder XRD patterns of white clayey antigorite (A6) and well-crystallized rock-forming antigorite (A1).

squares method. Estimated standard deviations are a 0.002 – 0.017, b 0.001 – 0.005, c 0.0001 – 0.002 Å, β 0.003 – 0.03°.

SAED patterns (Fig. 2) show a wider range of A parameters, from 28 to 61 Å (M 5.0 – 11.4, $M = A/a$; see Uehara & Shirozu 1985, Uehara & Kamata 1994). The supercell (A) is as defined above, and the distribution of the A parameter obtained by powder XRD is given in Figure 3. Values of A between 40.0 and 42.5 Å commonly occur in southwestern Japan. These values are smaller than the originally described supercell of 43 Å antigorite (Aruja 1945, Zussman 1954, Kunze 1956).

Powder XRD patterns of the samples studied show sharp to very broad supercell (satellite) and subcell reflections (Fig. 4). Sample A1 is well-crystallized rock-forming antigorite, whereas A6 is poorly crystallized clayey material. No supercell reflections are found in the latter sample. Cell parameters of the sample could not be obtained by powder XRD because of lack of convergence in the least-squares calculation, although by the TEM, sample A6 show clear low-order and diffuse high-order satellite reflections. This indicates that some samples of antigorite may contain many defects, such as a polysomatic disorder and stacking faults. The supercell of antigorite with these defects cannot be measured by powder XRD.

The M values were determined using both SAED and XRD methods. SAED gives the M parameter for each micrograin. In contrast, XRD provides an M value derived from a statistical average of all grains of a given sample. The M values by powder XRD generally agree with the average M values by electron diffraction, as shown in Figure 5. The M values in this figure, except for sample A2, were described in Uehara & Shirozu (1985), and compiled here for comparison of XRD and SAED. Many samples of antigorite show a large standard deviation in M value obtained by the SAED method. Ten or more grains should be measured to get a statistical average of a given sample. Also the averaging effect of XRD explains the smaller range of A variation compared to that found by SAED or direct HRTEM imaging.

A new method for supercell measurement using powder XRD

XRD powder data may be used to estimate average values of M parameter. Figure 6 shows the XRD patterns. In the 2θ range between 10 to 15° (Cu$K\alpha$), the

TABLE 1. CELL PARAMETERS OF ANTIGORITE SAMPLES, AS OBTAINED BY X-RAY DIFFRACTION

Antigorite samples from Nomo

	P14b	P26b	P34	P37	P17-3	P17-1	P1	P102	P17-2	P22	P13-2b	P30b	P20	P3
a (Å)	5.419	5.418	5.427	5.416	5.435	5.434	5.441	5.438	5.437	5.441	5.448	5.448	5.454	5.450
b (Å)	9.242	9.238	9.246	9.241	9.251	9.244	9.256	9.251	9.244	9.253	9.252	9.253	9.251	9.259
c (Å)	7.279	7.269	7.264	7.272	7.265	7.272	7.257	7.260	7.272	7.259	7.259	7.264	7.265	7.253
β (°)	91.22	91.17	91.19	91.08	91.22	91.30	91.13	91.18	91.29	91.26	91.34	91.34	91.43	91.27
V_{sub} (Å^3)	364.5	363.8	364.5	363.9	365.2	365.2	365.4	365.1	365.4	365.4	365.8	366.1	366.4	365.7
M	9.07	8.99	8.51	8.46	8.03	7.94	7.75	7.74	7.69	7.47	7.40	7.25	7.13	7.00
A (Å)	49.15	48.69	46.17	45.81	43.63	43.18	42.19	42.08	41.83	40.63	40.31	39.50	38.88	38.15

Antigorite samples from Bessi

	B20	B28b	B28c	B32a	B8	B13	B37	B44	B40	B49	B41	B50	B33	B2
a (Å)	5.421	5.424	5.426	5.432	5.430	5.443	5.440	5.442	5.445	5.449	5.447	5.452	5.466	5.456
b (Å)	9.247	9.240	9.248	9.247	9.248	9.250	9.252	9.256	9.255	9.254	9.245	9.242	9.253	9.250
c (Å)	7.260	7.265	7.265	7.261	7.266	7.262	7.261	7.250	7.270	7.243	7.258	7.249	7.253	7.262
β (°)	91.16	91.19	91.19	91.25	91.28	91.28	91.33	91.18	91.37	91.30	91.42	91.37	91.38	91.43
V_{sub} (Å^3)	363.9	364.0	364.5	364.5	364.8	365.5	365.4	365.1	366.3	365.1	365.4	365.2	366.7	366.4
M	9.06	8.93	8.66	8.47	8.22	8.11	7.97	7.84	7.48	7.21	7.15	7.00	6.93	6.81
A (Å)	49.11	48.44	46.99	46.01	44.63	44.14	43.36	42.67	40.73	39.29	38.95	38.16	37.88	37.16

Antigorite samples from	Oeyama	Ube	Kochi	Nishisonogi		Sasaguri
	S7*	S16	S35	N26	N55E	A2
a (Å)	5.446	5.426	5.447	5.441	5.461	5.455
b (Å)	9.248	9.253	9.239	9.247	9.256	9.253
c (Å)	7.254	7.276	7.253	7.268	7.266	7.266
β (°)	91.33	91.33	91.42	91.47	91.27	91.46
V_{sub} (Å^3)	365.3	365.2	364.8	365.5	367.2	366.6
M	7.52	8.86	7.16	8.23	6.58	6.92
A (Å)	40.95	48.02	38.66	44.13	35.93	37.75

* Uehara & Shirozu (1985)

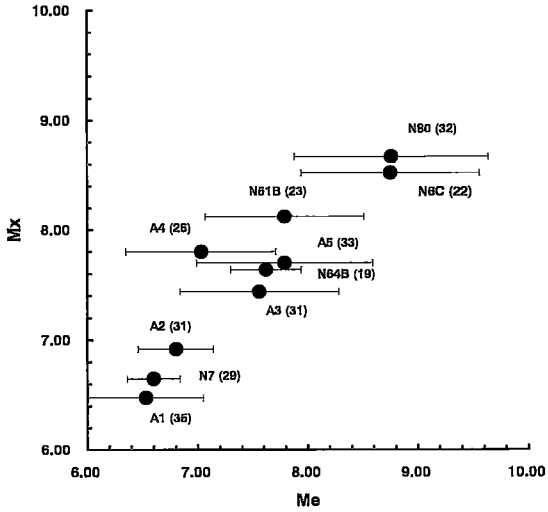

FIG. 5. Comparison of M values of antigorite obtained by electron-diffraction method (Me) and powder XRD method (Mx).

first to third-order satellite reflections (*e.g.*, where $h_s = 0 \pm u/M$ and $u = 1, 2$, or 3, the order of the h superlattice reflection, h_s) are observed near the 001 reflection. The difference in the 2θ angle between $h_s kl$: $0 \pm 3/M$, 0, 1 (Cu$K\alpha$) and 001 (Cu$K\beta$) reflections, Δ2θ, is caused by the variation in the supercell A parameter, or M value, because the c and β parameters are relatively constant over the 60 specimens (Table 1 of this study and Figure 5 of Uehara & Kamata 1994).

The Δ2θ values for antigorite from Nishisonogi and Sasaguri are plotted against M values in Figure 7. The M values are found to correlate with Δ2θ according to the following linear equation,

$$M = 14.26 - 2.41\ \Delta 2\theta \qquad (1)$$

Its correlation factor is 0.985. Thus the M value is easily obtained by the Δ2θ measurement using XRD; hereafter we refer to this as the Δ2θ method. This equation is recalculated for use with the 001 (Cu$K\alpha$) reflection instead of the 001 (Cu$K\beta$) reflection in the case of powder diffractometers with monochromators:

$$M = 11.42 - 2.41\ \Delta 2\theta \qquad (2)$$

Because of its simplicity, the technique was applied to a regional survey of antigorite superstructure.

The frequency distribution of M values obtained for 63 specimens of antigorite from Nishisonogi using the Δ2θ method are shown in Figure 8. The M parameter ranges from 6.6 to 8.9, with the maximum distribution at $M = 8.4$. This value of 8.4 is considered to be representative of the area, which was subjected to blueschist-facies metamorphism. The shape of the M value distribution in Figure 8 shows a tail toward smaller M values. The regional occurrence of the M parameter is plotted in Figure 9. The variation of M as found at Nishisonogi varies greatly, as it does in individual specimens. Thus, the metamorphic conditions (pressure and temperature) are relatively constant in this ultramafic body, whereas the M values show a heterogeneous distribution both macroscopically and microscopically. This indicates

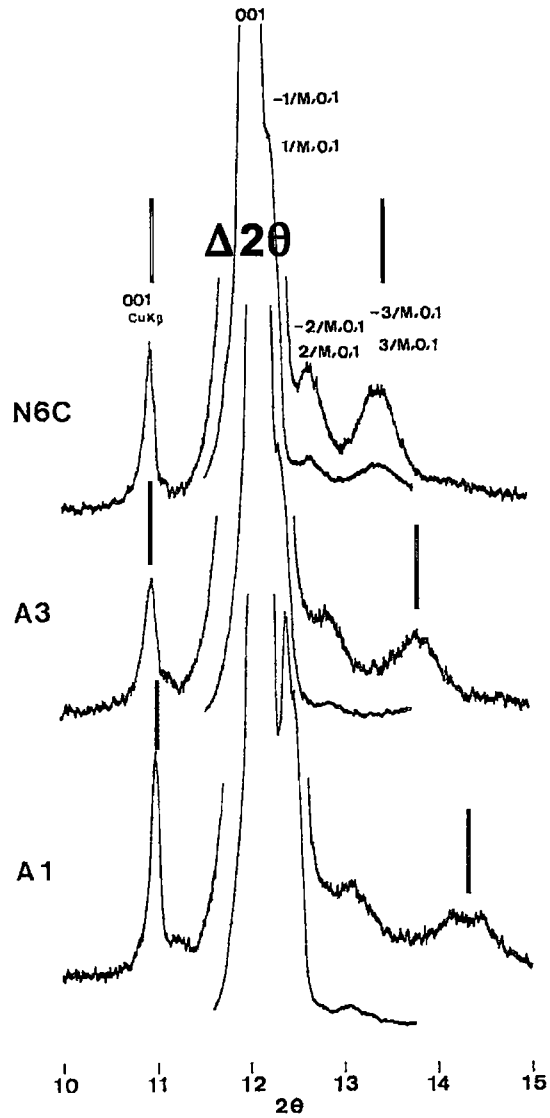

FIG. 6. Powder XRD patterns around 001 reflection of antigorite (sample N6C, A3, and A1). First- to third-order satellite reflections are observed.

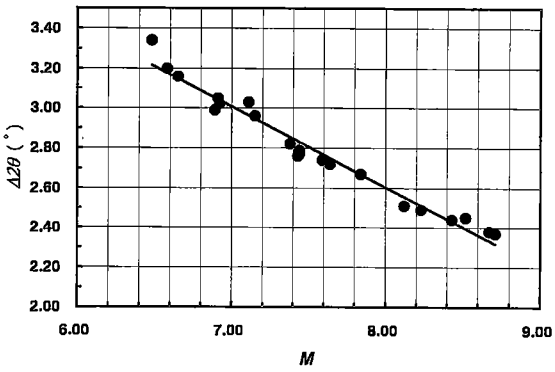

FIG. 7. Plots of $\Delta 2\theta = 2\theta\,(0 \pm 3/M, 0, 1\ \mathrm{Cu}K\alpha) - 2\theta\,(001\ \mathrm{Cu}K\beta)$ *versus* values of M in antigorite refined by powder XRD.

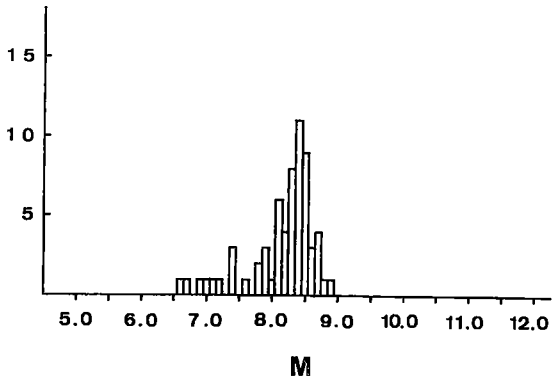

FIG. 8. A population of M values of the 63 samples of antigorite from Nishisonogi, obtained by the $\Delta 2\theta$ method.

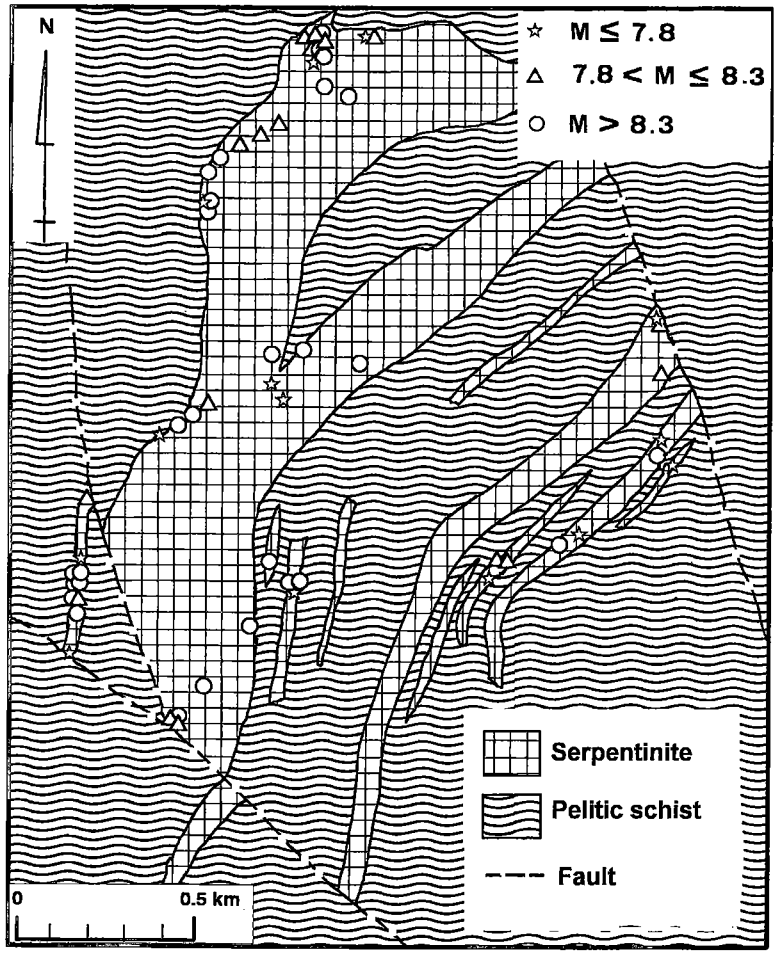

FIG. 9. Distribution of M values in antigorite from Nishisonogi obtained by the $\Delta 2\theta$ method. Geological map is simplified from Noda & Muta (1959).

that M values do not necessarily correspond to metamorphic grade.

The distribution of M values is more homogeneous in antigorite with smaller M values than in that with larger M values, as seen in Figure 3 of Uehara & Shirozu (1985). This suggests that equilibrium is more easily attained in the Nishisonogi antigorite with small M values, whereas it is not attained in antigorite with a large M value. Alternatively, there may be a slight difference in free energy among antigorite polysomes with larger M.

HRTEM images

Previously, HRTEM images of antigorite obtained along [001] were not investigated, because the 3 to 4 Å point-to-point resolution gives 4.6 Å fringes (corresponding to 020 and 110 reflections). Thus there is no atomic-scale structural information (Uehara 1994). However, the JEM–4000EX HRTEM used here has a better than 2 Å point-to-point resolution. Unfortunately, a through-focus series of images could not be recorded owing to rapid damage to the sample by the electron beam. Some HRTEM images of antigorite and serpentinite were shown in Uehara (1994).

The images of antigorite (A1) obtained down [001] are divided into two types (Fig. 10). The first type shows continuous (200) and discontinuous (130) fringes having a spacing of 2.5 Å. The offsets in the (130) fringe occur at arrows (Fig. 10a) at 35 Å separation. The supercell periodicity corresponds to M = 6.5. The second type shows (110) and (020) fringes of 4.6 Å spacing and similar offsets in the (110) fringe at 35 Å separation (Fig. 10b). The difference between the two types is related to the focus condition and thickness, which are shown in simulated images (see below).

To interpret these images, HRTEM images were calculated using the computer program CIHRTEM of Horiuchi & Matsui (1983). Calculations were made for different thicknesses of the crystal, 36.4, 72.8, 145.6, and 291.2 Å, with defocus values from –200 to 1000 Å. Selected results of the simulated HRTEM image of antigorite with M = 8.0 are shown in Figure 11.

The simulated images show that the offsets in the pattern of (110) and (130) fringes are found at 8-ring reversals and not at 6-ring reversals. In calculated through-focus images, such offsets are seen under a wide range of defocus conditions and sample thickness. In [001] HRTEM images, 6- and 8-ring reversal modules are clearly distinguishable. The HRTEM images of antigorite having M = 6.5 show ordering of 6- and 8-ring reversal modules along the supercell (Fig. 10b). This indicates that the type of supercell with M = $(2n + 1)/2$ requires doubling the A value, as formed in a

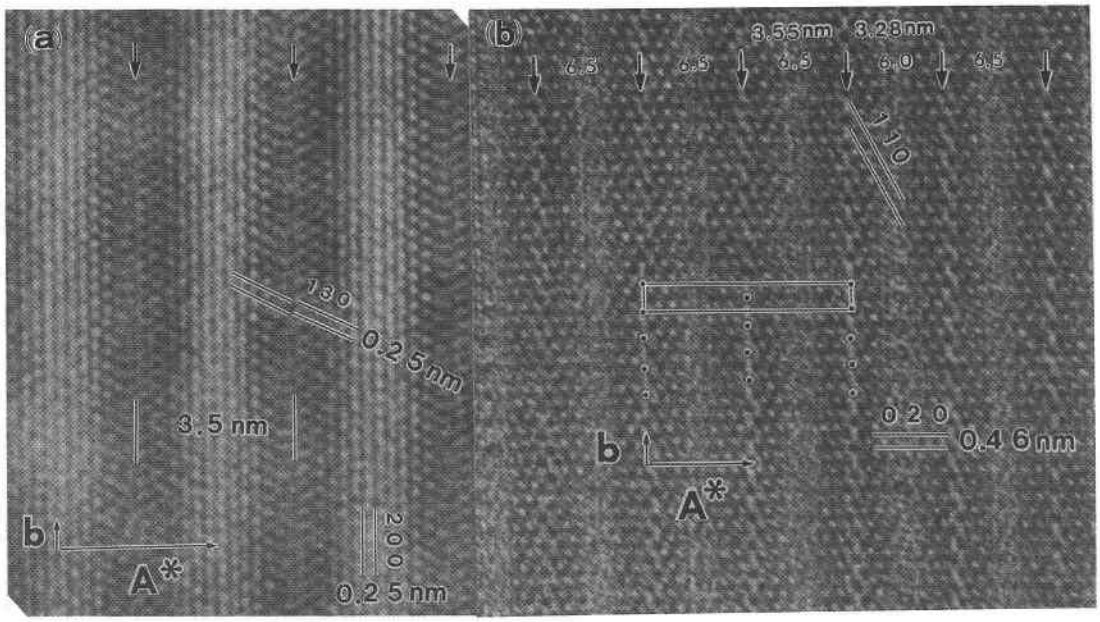

FIG. 10. HRTEM image of antigorite sample A1 viewed along [001], obtained with a JEM–4000EX instrument. Arrows indicate the 8-ring reversal. (a) Strong (130) and (200) fringes are observed (110) fringe shows offset at 8-ring reversal. (b) Strong (110) and (020) fringes are observed; (110) fringe shows at 8-ring reversal. Black dots correspond to 8-membered ring. *C*-centered lattice is also shown.

TABLE 2. ATOMIC PARAMETERS OF ANTIGORITE, USING HRTEM IMAGE CALCULATIONS

Mg	0.031 0.000 0.519	Si	0.057 0.167 0.139	OH	0.070 0.000 0.714	O	0.179 0.167 0.408	O	0.885 0.000 0.909
Mg	0.031 0.333 0.519	Si	0.117 0.333 0.164	OH	0.196 0.000 0.750	O	0.056 0.167 0.370	O	0.943 0.500 0.945
Mg	0.094 0.167 0.548	Si	0.177 0.167 0.180	OH	0.324 0.000 0.743	O	0.518 0.167 0.652	O	0.058 0.000 0.048
Mg	0.094 0.500 0.548	Si	0.237 0.333 0.187	OH	0.451 0.000 0.693	O	0.821 0.333 0.593	O	0.117 0.500 0.078
Mg	0.156 0.000 0.571	Si	0.299 0.167 0.189	OH	0.867 0.000 0.267	O	0.578 0.333 0.615	O	0.175 0.000 0.096
Mg	0.156 0.333 0.571	Si	0.358 0.333 0.185	OH	0.613 0.000 0.271	O	0.944 0.333 0.630	O	0.238 0.500 0.104
Mg	0.219 0.167 0.583	Si	0.418 0.167 0.164	OH	0.740 0.000 0.250	O	0.117 0.333 0.391	O	0.297 0.000 0.109
Mg	0.219 0.500 0.583	Si	0.477 0.333 0.123	OH	0.007 0.167 0.667	O	0.995 0.333 0.328	O	0.356 0.500 0.100
Mg	0.282 0.000 0.583	Si	0.523 0.167 0.878	OH	0.133 0.167 0.733	O	0.699 0.333 0.590	O	0.414 0.000 0.076
Mg	0.282 0.333 0.583	Si	0.582 0.333 0.836	OH	0.260 0.167 0.750	O	0.883 0.167 0.609	O	0.472 0.500 0.035
Mg	0.344 0.167 0.575	Si	0.642 0.167 0.815	OH	0.388 0.167 0.729	O	0.362 0.333 0.399	O	0.529 0.000 0.970
Mg	0.344 0.500 0.575	Si	0.701 0.333 0.811	OH	0.804 0.167 0.250	O	0.301 0.167 0.410	O	0.588 0.500 0.936
Mg	0.407 0.000 0.563	Si	0.763 0.167 0.813	OH	0.549 0.167 0.307	O	0.482 0.333 0.348	O	0.647 0.000 0.910
Mg	0.407 0.333 0.563	Si	0.823 0.333 0.820	OH	0.676 0.167 0.259	O	0.240 0.333 0.414	O	0.708 0.500 0.900
Mg	0.468 0.167 0.533	Si	0.883 0.167 0.836	OH	0.930 0.167 0.286	O	0.760 0.167 0.586	O	0.768 0.000 0.893
Mg	0.468 0.500 0.533	Si	0.943 0.333 0.861	OH	0.070 0.333 0.714	O	0.639 0.167 0.601	O	0.827 0.500 0.893
Mg	0.532 0.000 0.481	Si	0.999 0.333 0.089	OH	0.196 0.333 0.750	O	0.422 0.167 0.385	O	0.000 0.500 0.000
Mg	0.532 0.333 0.481	OH	0.117 0.000 0.391	OH	0.324 0.333 0.741			O	0.088 0.250 0.064
Mg	0.594 0.167 0.452	OH	0.240 0.000 0.414	OH	0.451 0.333 0.693			O	0.147 0.250 0.090
Mg	0.594 0.500 0.452	OH	0.362 0.000 0.399	OH	0.867 0.333 0.267			O	0.208 0.250 0.100
Mg	0.656 0.000 0.429	OH	0.482 0.000 0.348	OH	0.613 0.333 0.271			O	0.268 0.250 0.107
Mg	0.656 0.333 0.429	OH	0.578 0.000 0.615	OH	0.740 0.333 0.250			O	0.327 0.250 0.107
Mg	0.718 0.167 0.417	OH	0.699 0.000 0.590	OH	0.007 0.500 0.667			O	0.385 0.250 0.091
Mg	0.718 0.500 0.417	OH	0.821 0.000 0.593	OH	0.133 0.500 0.733			O	0.443 0.250 0.055
Mg	0.781 0.000 0.417	OH	0.944 0.000 0.630	OH	0.260 0.500 0.750			O	0.500 0.250 0.000
Mg	0.781 0.333 0.417	OH	0.995 0.000 0.328	OH	0.388 0.500 0.729			O	0.558 0.250 0.952
Mg	0.844 0.167 0.425	OH	0.056 0.500 0.370	OH	0.804 0.500 0.250			O	0.617 0.250 0.923
Mg	0.844 0.500 0.425	OH	0.179 0.500 0.408	OH	0.549 0.500 0.307			O	0.678 0.250 0.904
Mg	0.906 0.000 0.438	OH	0.301 0.500 0.410	OH	0.676 0.500 0.259			O	0.738 0.250 0.896
Mg	0.906 0.333 0.438	OH	0.422 0.500 0.385	OH	0.930 0.500 0.286			O	0.797 0.250 0.891
Mg	0.969 0.167 0.467	OH	0.518 0.500 0.652					O	0.856 0.250 0.900
Mg	0.969 0.500 0.467	OH	0.639 0.500 0.601					O	0.914 0.250 0.924
		OH	0.760 0.500 0.586					O	0.972 0.250 0.965
		OH	0.883 0.500 0.609					O	0.029 0.250 0.030

$A = 43.3$ Å, $b = 9.23$ Å, $c = 7.27$ Å, $\beta = 91.6°$, space group *Pm*.

C-cell lattice. Most calculated [001] images of antigorite exhibit dots with higher contrast, corresponding to the positions of Si atom [*i.e.*, black dots in Fig. 11(2)], or to the positions of Si and inner OH [*i.e.*, white dots in Fig. 11(3)]. The white dots in the experimental image (Fig. 10a) correspond to the Si and inner OH atomic positions. Although calculated images could not be compared to a through-focus series, the data presented here strongly suggest the exitence of the *C*-cell model as proposed by Uehara & Shirozu (1985).

The [001] HRTEM image of sample A5 resembles that of sample A1, but there are differences in detail; the (200) fringe is relatively sharp, and (130) fringe is diffuse. This pattern implies a stacking fault along the *b*-axis parallel to the projected plane. Such defects are shown in images viewed down [010] and [100].

An additional type of antigorite superstructure was observed by TEM. This new structure is a one-layer structure with a larger β, equal to 95°, which corresponds to a layer shift along the *X* axis of –0.64 Å (Uehara 1995). Therefore, different kinds of structural distortions exist in antigorite. Details of the HRTEM results will be presented elsewhere (Uehara, in prep.).

ACKNOWLEDGEMENTS

I thank Professors Y. Aoki, I. Shinno, and M. Matsui of Kyushu University for helpful comments and discus-

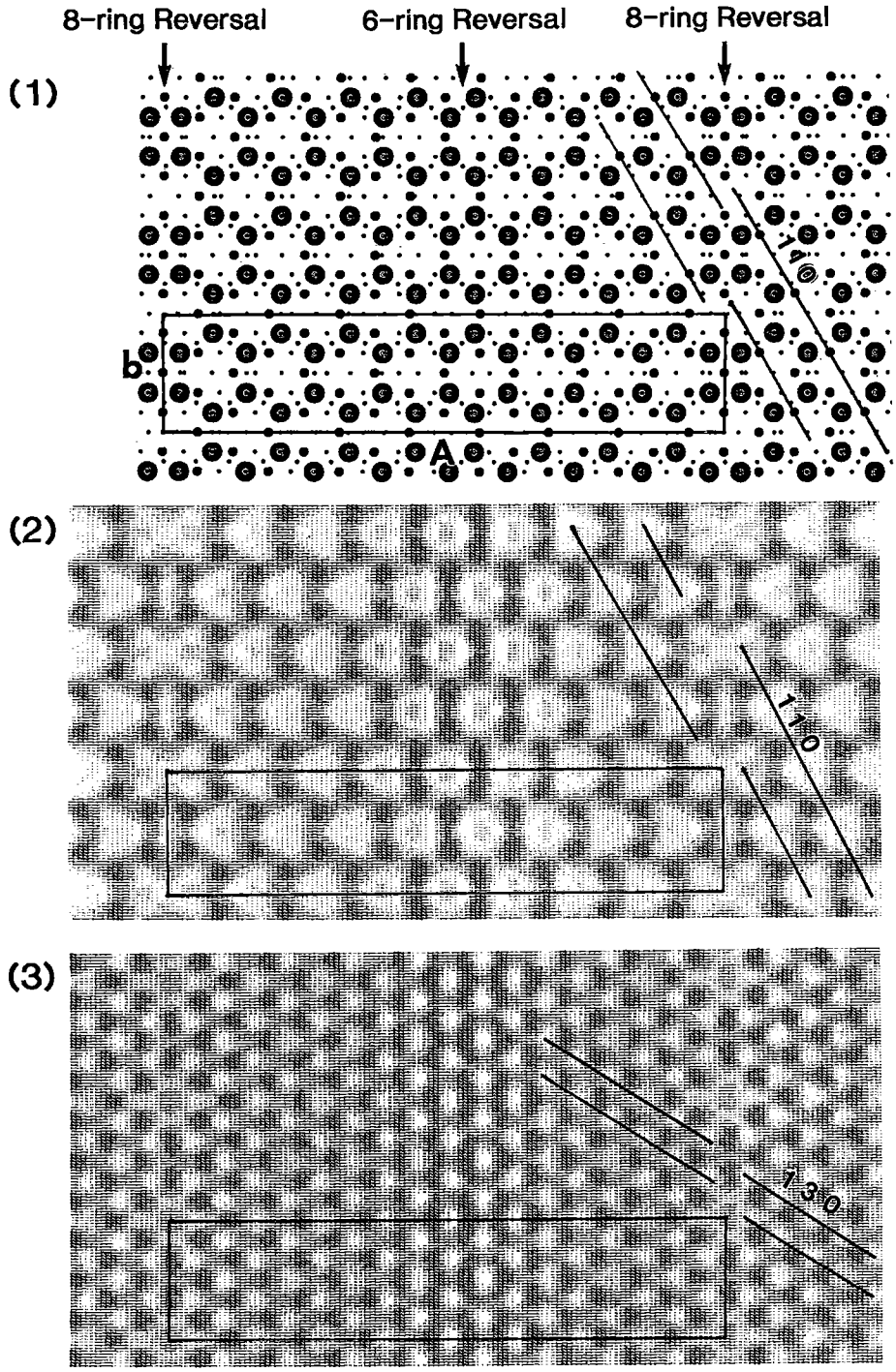

FIG. 11. Simulated *c*-axis images of $M = 8.0$ antigorite, (1) Model of the structure (modified from Kunze 1956, 1958). (2), (3) Calculated images using the parameters as follows. Defocus of 400 Å for (2), 0 Å for (3), thickness 36.4 Å, spherical aberration coefficient of 1.0 mm and beam convergence of 0.5 mradian.

sions. Emeritus Professor Haruo Shirozu of Kyushu University is acknowledged for supporting much of this research. Mr. K. Ito and Mr. T. Nishi assisted in experiments and collection of samples. We are grateful to Drs. S. Guggenheim, A. Baronnet, and an anonymous referee for constructive reviews, and to Drs. R.F. Martin and H. Vali for editorial assistance. This research was supported by a Grant-in-Aid for Scientific Research from the Ministry of Education, Science, and Culture, Japan (C2, 07640645).

References

ARUJA, E. (1945): An X-ray study of the crystal structure of antigorite. *Mineral. Mag.* **27**, 65-74.

HASHIMOTO, M., IGI, S., SEKI, Y., BANNO, S. & KOJIMA, G. (1970): Notes on metamorphic facies map of Japan. *Geol. Survey Japan.*

HORIUCHI, S. & MATSUI, Y. (1983): Crystal structure images by high-resolution transmission electron miroscopy. *J. Crystallogr. Soc. Jap.* **25**, 3-20 (in Japanese).

KUNZE, G. (1956): Die gewelte Struktur des Antigorits, I. *Z. Kristallogr.* **108**, 82-107.

_____ (1958): Die gewelte Struktur des Antigorits, II. *Z. Kristallogr.* **110**, 282-320.

_____ (1961): Antigorite. Strukturtheoretishe Grundlagen und ihre praktische Bedeutung für die weitere Serpentin-Forschung. *Fortschr. Mineral.* **39**, 206-324.

MELLINI, M., TROMMSDORFF, V. & COMPAGNONI, R. (1987): Antigorite polysomatism: behavior during progressive metamorphism. *Contrib. Mineral. Petrol.* **97**, 147-155.

MIYASHIRO, A. (1961): Evolution of metamorphic belts. *J. Petrol.* **2**, 277-311.

NODA, M. & MUTA, K. (1959): The geological structure of the Nishisonogi Peninsula, Nagasaki Prefecture. *Rep. Earth Science College of General Education, Kyushu Univ.* **4**, 17-21.

OTTEN, M.T. (1993): High-resolution transmission electron microscopy of polysomatism and stacking defects in antigorite. *Am. Mineral.* **78**, 75-84.

SPINNLER, G.E. (1985): *HRTEM Study of Antigorite, Pyroxene-Serpentine Reactions, and Chlorite.* Ph.D. dissertation, Arizona State Univ., Tempe, Arizona.

UEHARA, S. (1987): Serpentine minerals from Sasaguri area, Fukuoka Prefecture, Japan. *J. Jap. Assoc. Mineral., Petrol. Econ. Geol.* **82**, 106-118 (in Japanese with English abstr.).

_____ (1994): Transmission electron microscopy applied to the studies of sheet silicates and related minerals. *Koubutugaku Zasshi (J. Mineral. Soc. Japan)* **23**, 111-125 (in Japanese with English abstr.).

_____ (1995): *Superstructure and Crystal Chemistry of Antigorite.* Ph.D. dissertation, Kyushu University, Fukuoka, Japan.

_____ & KAMATA, K. (1994): Antigorite with a large supercell from Saganoseki, Oita Prefecture, Japan. *Can. Mineral.* **32**, 93-103.

_____ & SHIROZU, H. (1985): Variations in chemical composition and structural properties of antigorites. *Mineral. J.* **12**, 299-318.

WHITTAKER, E.J.W. & ZUSSMAN, J. (1956): The characterization of serpentine minerals by X-ray diffraction. *Mineral. Mag.* **31**, 107-126.

WICKS, F.J. & WHITTAKER, E.J.W. (1975): A reappraisal of the structures of the serpentine minerals. *Can. Mineral.* **13**, 227-243.

ZUSSMAN, J. (1954): Investigation of the crystal structure of antigorite. *Mineral. Mag.* **30**, 498-512.

_____, BRINDLEY, G.W. & COMER, J.J. (1957): Electron diffraction studies of serpentine minerals. *Am. Mineral.* **42**, 133-153.

Received October 15, 1997, revised manuscript accepted July 8, 1998.